JOURNAL OF COLLOID AND INTERFACE SCIENCE **202,** 173–188 (1998)
ARTICLE NO. CS985448

Simulation of Droplet Motion on Low-Energy and Heterogeneous Surfaces

Leonard W. Schwartz*,[1] and Richard R. Eley†

**Departments of Mechanical Engineering and Mathematical Sciences, The University of Delaware, Newark, Delaware 19716; and †The Glidden Research Laboratory, ICI Paints, Strongsville, Ohio 44136*

Received October 7, 1997; accepted January 29, 1998

A method of calculation is introduced that allows the simulation of the time-dependent three-dimensional motion of liquid droplets on solid substrates for systems exhibiting finite equilibrium contact angles. The contact angle is a prescribed function of position on the substrate. An evolution equation is presented, using the lubrication approximation, that includes viscous, capillary, disjoining, and gravitational forces. Motion to and from dry substrate regions is made possible by use of a thin energetically stable wetting layer. Axisymmetric spreading on a uniform substrate is calculated, and it is found, in agreement with reported experiments, that spreading rates are independent of the contact angle until the drop has almost stabilized. We simulate motion on a heterogeneous substrate composed of two different materials having widely different contact angles. Motion proceeds in an almost discontinuous fashion as the initial droplet breaks up into smaller pieces through the action of the wetting forces. Various forms of the disjoining energy functional are employed; the particular choice is found to have only a limited quantitative effect of the drop dynamics. Experimental observations confirm the basic features of the simulation, although a time-scale correction needs to be applied.

Key Words: **Droplet spreading; heterogeneous substrate; numerical simulation; surface tension; disjoining pressure; fluid mechanics.**

1. INTRODUCTION

We are concerned with the slow motion of droplets on solid surfaces. So-called high-energy surfaces are those for which a droplet of finite lateral extent, of a given liquid, will not persist for long times; rather the droplet will spread, under the action of surface forces, until the contact angle, at the three-phase line, where substrate, liquid, and vapor meet, is effectively equal to zero. In many common situations, on the other hand, static droplets, with a well-defined nonzero contact angle can be observed. These may be termed low-energy or partially wetting systems. Sometimes this contact angle, for a static drop, will depend on the previous history of the drop motion, a phenomenon known as contact angle hysteresis. Contact angle hysteresis is believed to be caused by substrate heterogeniety which may be either physical (i.e., microscopic roughness) or chemical, if the substrate is contaminated by small patches of a solid coating having a different equilibrium contact angle, for example. For a moving drop, observed contact angles also depend on the speed of the motion, and one often refers to dynamic (i.e., advancing and receding) contact angles (1). Interesting and practically important issues arise concerning the relative importance of interface-energetic versus dynamic effects in wetting/dewetting phenomena.

In this paper we demonstrate the feasibility of time-dependent numerical simulation of droplet spreading on heterogeneous surfaces. The so-called lubrication or long-wave approximation is used in the simulations. This approximation has been shown to be a valid simplication of the Navier–Stokes equations of viscous flow when used to model the slow motion of liquid layers, provided the liquid free-surface slope is sufficiently small (2–4). A single partial differential equation in space and time describes the evolving liquid surface and surface tension, gravitational, and other effects can be incorporated. For two-dimensional or axisymmetric problems, the solution $h(x, t)$ or $h(r, t)$ involves only a single spatial coordinate, while solutions of three-dimensional problems are of the form $h(x, y, t)$ where x and y are the substrate coordinates.

For a partially wetting system, the shape of statically stable liquid droplets can be represented mathematically using the Frumkin–Deryaguin model (5–7). The substrate region near the margin of the macroscopic droplet is covered with a submicroscopic layer of wetting liquid. This wetting layer is maintained in a state of stable equilibrium through the action of intermolecular forces. There is excess or ''disjoining'' pressure in the thin film that arises from a variety of causes; these contributions are often divided into molecular, ionic-electrostatic, and structural components. A useful survey of the substantial theoretical and experimental literature

[1] To whom correspondence should be addressed.

0021-9797/98 $25.00

on disjoining pressure is given by Mohanty (8). In the contact region, the condition of constancy of total pressure, including capillary and disjoining components, determines the shape of the liquid–vapor interface. The apparent contact angle, or maximum slope of the interface, may be found as a function of the surface tension and the parameters in the expression used for the disjoining pressure.

The existence of the wetting layer serves another purpose for dynamic simulations. The lubrication formulation, like the full Navier–Stokes problem from which it is derived, does not allow liquid motion to or from perfectly dry regions of the substrate. The difficulty lies in the incompatibility between the usual no-slip condition, where the moving liquid meets the substrate, and the boundary conditions on the liquid–vapor interface, leading to a nonintegrable force singularity where these two interfaces meet at the contact line (9). The thin wetting layer alleviates this problem and is an alternative to the slip models otherwise used in dynamic studies (10, 11). Asymptotic analyses of spreading using a thin wetting layer are given by Tanner (12) and Tuck and Schwartz (13). Experimental data for the speed of spreading drops in various systems suggests that the wetting layer thickness, h_* say, lies in the broad range of 1 to 100 nm (12, 14, 15). A number of dynamic studies, using various forms of the disjoining pressure term in a two-dimensional or axisymmetric lubrication model for wetting/dewetting, have also appeared (15–20).

In the next section, we present the lubrication model for three-dimensional unsteady motion of droplets on heterogeneous substrates. A two-term disjoining pressure model with a single stable energy minimum is used. The contact angle is taken to be an arbitrary function of the substrate coordinates (x, y). It is shown that the overall rate of viscous dissipation is equal simply to the rate of decrease of the stored energy components; the latter may be subdivided into free-surface, substrate or disjoining, and gravitational components. Thus episodes of rapid motion can be associated with rapid decrease of stored energy since viscous dissipation varies as the square of the velocity of motion. A degree of dynamic similarity is revealed through the introduction of dimensionless variables. The viscosity, surface tension, and equilibrium contact angle of a droplet on a reference substrate can all be absorbed into the units of space and time.

Section 3 gives details of the numerical techniques employed for solving the evolution equation. The margins of moving droplets are ''captured'' by the numerical scheme and thus appear naturally as part of the solution without the necessity of fitting their positions. Section 4 then gives simulation results for a relatively simple problem: the axisymmetric spreading of a drop on a partially wetting substrate. It is demonstrated that drops spread according to a universal law, even when the contact angle is finite. Only as the drop nears its final configuration does the partially wetting character of the system influence the motion. This is consistent with experimental measurements of Zosel (21) who observed this invariance for various finite-contact-angle systems. The principal determinant of the drop-spreading rates is the wetting layer thickness h_*. The numerical results are compatible with the theoretical prediction that instantaneous spreading speeds should vary inversely as the logarithm of h_* (12, 13, 22). Comparison of the numerical results with experimental data identifies the actual value of h_* for a particular system. It is possible to use realistically small values of h_* in two-dimensional and axisymmetric simulations. The mesh size must be made smaller as h_* is reduced however in order to produce numerically accurate results. For three-dimensional simulations, the mesh extends in both substrate directions, and very many more mesh ''blocks'' are needed. It is not computationally feasible to use very small values of h_*, and a time scale correction needs to be applied to compensate for the overly large value of h_*.

Section 5 describes the simulation of a droplet moving on a particular pattern of wettability. The pattern is chosen to match experimental results that are also given in the section. The drop is placed initially near the center of a cross of poorly wetting material that had been applied to an otherwise uniform substrate. Wetting forces cause the droplet to break up, with fragments of various sizes remaining in each of the four quadrants. Details of the motion and the sequence of breaking events is well modeled by the simulation. Three different forms of the disjoining pressure function are used in the simulation corresponding to different disjoining energy ''well'' shapes. While each choice gives roughly similar behavior, the differences can be explained in terms of the ''stiffness'' of the drop as it moves and deforms. An additional simulation is presented with gravity included in order to ascertain its effect. For the conditions of the experiment, especially the drop size, gravity is shown to be relatively unimportant. Relevant experimental parameters are given in Section 5.

The final section outlines extensions of the present work. It is suggested that the simulation capability can be used as an aid in the quantitative understanding of wetting forces when used in conjunction with suitably designed experiments. Direct modeling of the origins of contact angle hysteresis, and its dependence on particular wettability patterns, can also be probed.

2. THE LUBRICATION EVOLUTION EQUATION AND ENERGETICS FOR PARTIALLY WETTING SYSTEMS

For definiteness we consider a layer of liquid, or an isolated droplet, on a plane substrate inclined to the horizontal at an angle θ. A right-handed triad with the x and y axes

lying on the substrate is formed by x, y, and z where x is increasing in the uphill direction. The liquid surface corresponds to $z = h(x, y, t)$ where t is time.

In three dimensions, integral mass conservation and the creeping-motion force balance can be combined to yield the evolution equation

$$h_t = -\nabla \cdot \mathbf{Q} = \frac{1}{3\mu} \nabla \cdot (h^3 \nabla p) \qquad [2.1a]$$

where

$$p = -\sigma \nabla^2 h - \Pi + \rho g h \cos\theta + \rho g x \sin\theta. \qquad [2.1b]$$

Here σ is surface tension, ρ is density, and g is the acceleration of gravity. $\mathbf{Q}$ is an areal flux vector with dimensions $[L^2/T]$. $\nabla^2 h$ is the small-slope approximation to the free-surface curvature. Π is called the disjoining pressure and will be taken to be of the form

$$\Pi = \frac{B}{h_*^n} \left[\left(\frac{h_*}{h} \right)^n - \left(\frac{h_*}{h} \right)^m \right]. \qquad [2.2]$$

B and the exponents n and m are positive constants with $n > m > 1$. The first term represents liquid-solid repulsion, while the second is attractive, leading to a stable film thickness $h = h_*$.

With only the surface tension and gravity terms on the right side, Eq. [2.1] is well documented (2–4). It has been used, for example, to calculate the unsteady evolution of a liquid mound on a vertical wall as it slowly falls and forms ''drip marks'' (23). Its validity requires sufficiently slow motion so that the inertial terms in the Navier–Stokes equations may be neglected. In addition, the inclination of the liquid surface, relative to the substrate, must be small since terms of order $\nabla h \cdot \nabla h$ are neglected compared with terms of nominal order unity. The shear stress on the liquid free surface is zero and the pressure above the liquid is constant.

The two-term disjoining pressure used here establishes an energetically favored thin wetting layer on the substrate of height h_*. The stored energy per unit substrate area, if the wetting layer is displaced from h^* to h, is

$$\begin{aligned} e^{(d)}(h) &= -\int_{h_*}^{h} \Pi(h')\, dh' \\ &= \frac{B}{h_*^{n-1}} \frac{n-m}{(m-1)(n-1)} \\ &\quad \times \left[1 - \frac{n-1}{n-m} \left(\frac{h_*}{h} \right)^{m-1} + \frac{m-1}{n-m} \left(\frac{h_*}{h} \right)^{n-1} \right]. \end{aligned} \qquad [2.3]$$

The constant B may be replaced in favor of the equilibrium contact angle θ_e by assuming that h_* is very small and performing a force balance in the neighborhood of the apparent ''contact'' point. On a scale of h_*, the drop surface asymptotes to an inclination angle θ_e with the substrate for $h \gg h_*$. The force components toward the drop center are thus $\sigma \cos\theta$ from the liquid surface and $e^{(d)}(h \to \infty)$ arising within the liquid. These are balanced by the wetting-layer forces σ and $e^{(d)}(h_*) = 0$. Thus, for a static drop, we obtain

$$\begin{aligned} B &= h_*^{n-1} \frac{(n-1)(m-1)}{(n-m)} \sigma(1 - \cos\theta_e) \\ &\approx h_*^{n-1} \frac{(n-1)(m-1)}{2(n-m)} \sigma\theta_e^2 \end{aligned} \qquad [2.4]$$

when the small-slope approximation is used. Equation [2.4] has been obtained by Mitlin (24) for the particular case $(n, m) = (9, 3)$. For h approximately equal to h_*, the wetting film energetics are dominated by $d^2 e^{(d)}/dh^2$ evaluated at $h = h_*$ which gives the local shape of the ''energy well.'' From Eq. [2.3], we calculate

$$\left[\frac{d^2 e^{(d)}}{dh^2} \right]_{h=h_*} = \frac{\sigma\theta_e^2}{2h_*^2} (m-1)(n-1)$$

using the approximation in Eq. [2.4].

Dimensionless disjoining pressure functions $\hat{\pi} = \pi h_*/(\sigma\theta_e^2)$ and disjoining energy densities $\hat{e}^{(d)} = e^{(d)}/(\sigma\theta_e^2)$ are shown in Figs. 1a and 1b, respectively. The independent variable is h/h_*. The three curves shown in each figure correspond to the exponent pairs used in this study: (3, 2), (4, 3), and (9, 3). By using these three pairs, we seek to explore the effect of changes in this function that can be expected over a range of material systems. The pair (3, 2) is suggested by Teletzke *et al.* (17) while Mitlin and Petviashvili (19) give results of two-dimensional calculations using (9, 3). The pair (9, 3) is the result of volume integration of molecular forces arising from the well-known Lennard–Jones 6-12 potential. The intermediate case (4, 3) was used by us in preliminary three-dimensional calculations (25). The depth of the energy well in Fig. 1b will be seen to have an effect on the dynamics. The least severe case (3, 2) allows some mathematical simplification and is also a bit easier to use in the computations to follow. It allows slightly smaller values of h_* and will be used most frequently here. For the (3, 2) case, a simple closed-form solution can be found for the shape of the free surface near the contact point when the liquid is in equilibrium considering only disjoining and surface tension forces. Close to the contact point only

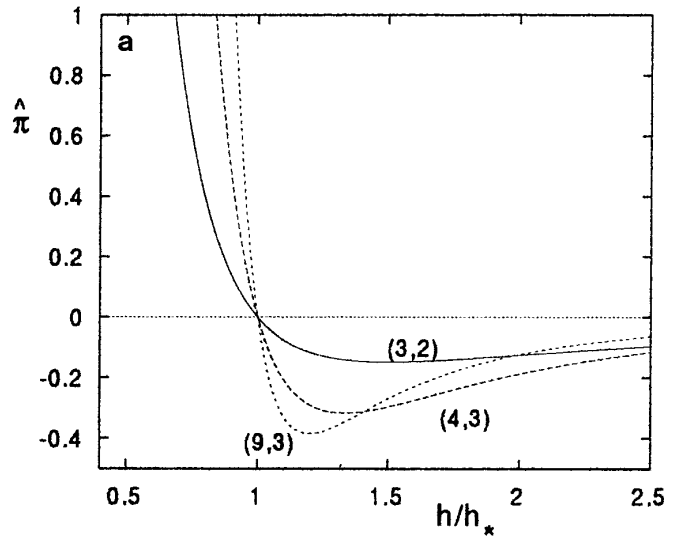

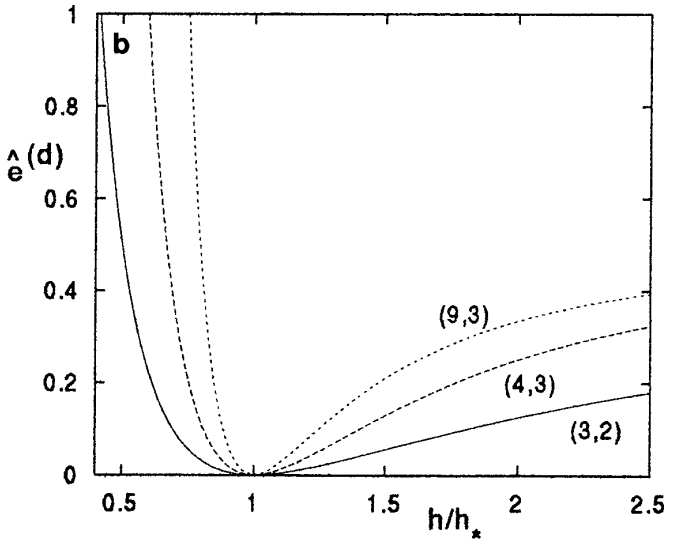

FIG. 1. (a) Nondimensional disjoining pressure $\hat{\pi} = \pi h_*/(\sigma\theta_e^2)$, and (b) disjoining energy density $\hat{e}^{(d)} = e^{(d)}/(\sigma\theta_e^2)$ plotted versus dimensionless layer height h/h_* for the three exponent pairs used in this study.

a two-dimensional problem needs to be considered. For small surface slope, the differential equation is

$$p = -h_{xx} - \Pi = 0.$$

For $(n, m) = (3, 2)$, this may be integrated twice, using $h_x \to \theta_e$ as $h \to \infty$, to obtain

$$\frac{h}{h_*} + \log\left(\frac{h}{h_*} - 1\right) = \pm\theta_e \frac{x - x_0}{h_*}. \qquad [2.5]$$

x_0 could be considered to be the ''contact point''; it corresponds to the specific value $h/h_* \approx 1.278\ \cdots$.

Each of the forces on the right of Eq. [2.1b] may be identified with an integrated energy component. The free-surface energy is proportional to the area of the liquid surface and is given by

$$E_1 = E^{(\sigma)} = \sigma \iint \left(\frac{1}{\cos\,\gamma} - 1\right) dA$$

where A is the total area of the substrate, and γ is the angle between the normal to the surface and the normal to the substrate. With the small slope assumption, it becomes

$$E_1 = E^{(\sigma)} \approx \frac{\sigma}{2} \iint \nabla h \cdot \nabla h dA. \qquad [2.6a]$$

The total disjoining energy is

$$E_2 = E^{(d)} = \iint e^{(d)} dA = \frac{\sigma}{2} \iint \times \theta_e^2 \left[1 + \frac{m-1}{n-m}\left(\frac{h_*}{h}\right)^{n-1} - \frac{n-1}{n-m}\left(\frac{h_*}{h}\right)^{m-1}\right] dA. \qquad [2.6b]$$

When $(n, m) = (3, 2)$, this takes the simpler form

$$E_2 = E^{(d)} = \iint e^{(d)} dA = \frac{\sigma}{2} \iint \theta_e^2 \left(1 - \frac{h_*}{h}\right)^2 dA.$$

The integrated gravitational energy components are

$$E_3 = E^{(g_s)} = \rho g \sin\theta \iint x(h - h_*) dA \qquad [2.6c]$$

and

$$E_4 = E^{(g_n)} = \frac{1}{2} \rho g \cos\theta \iint (h^2 - h_*^2) dA. \qquad [2.6d]$$

Each of the components $E_1, \ldots, E_4$ represents a stored or potential energy and is inherently positive as defined. The reference or zero-energy state for each of the components is a uniform liquid layer at the wetting-layer equilibrium height h_*. Note that E_3 is proportional to the *centroid* of the liquid volume

$$x_c = \frac{\iint x(h - h_*) dA}{\iint (h - h_*) dA}. \qquad [2.7]$$

For a paraboloidal drop of central height h_0 and radius R_0, that is,

$$h = h_* + h_0(1 - r^2/R_0^2)$$

for $r < R_0$ and $h = h_*$ for $r > R_0$, placed on a substrate of constant contact angle θ_e, the surface and disjoining energy components are given approximately as

$$E^{(\sigma)} \approx \pi\sigma h_0^2 \qquad [2.8a]$$

and

$$E^{(d)} \approx 2\pi\sigma h_0^2 \qquad [2.8b]$$

where the relation

$$\theta_e \approx \frac{2h_0}{R_0}$$

has been used. Note that the energies in Eqs. [2.8] are independent of R_0.

The rate of viscous dissipation over the entire substrate is

$$\dot{E}^{(\mu)} = -\iint \mathbf{Q}\cdot\nabla p dA = \iint p\nabla\cdot\mathbf{Q} dA = -\iint p h_t dA \qquad [2.9]$$

where the divergence theorem has been used in obtaining the second equality and $\mathbf{Q}$ is taken to be $\mathbf{0}$ on the boundaries of the domain A. The last form follows from the continuity equation [2.1a]. Replacing the effective pressure p using [2.1b] expresses $\dot{E}^{(\mu)}$ as a sum of four integrals. These are

$$-\dot{E}_1 = \sigma \iint h_t\nabla^2 h dA = \sigma \iint [\nabla\cdot(h_t\nabla h) - \nabla h_t\cdot\nabla h] dA.$$

Here, again using the divergence theorem and taking $\nabla h\cdot\mathbf{n} = 0$ on the edges of the domain to eliminate the first term on the right, we obtain

$$-\dot{E}_1 = -\frac{\sigma}{2}\frac{d}{dt}\iint \nabla h\cdot\nabla h dA = -\frac{dE^{(\sigma)}}{dt}. \qquad [2.10a]$$

Similarly, the disjoining energy term becomes

$$-\dot{E}_2 = \iint \Pi h_t dA = -\iint \frac{de^{(d)}}{dh} h_t dA = -\frac{d}{dt}\iint e^{(d)} dA = -\frac{dE^{(d)}}{dt} \qquad [2.10b]$$

where $E^{(d)}$ is given for general values of (n, m) in Eq. [2.6b].

The time rates of change of the two integrated gravitational energy components, formed by inserting the last two terms in Eq. [2.1b] into the integrand in Eq. [2.9], are easily shown to satisfy

$$-\dot{E}_3 = -\frac{dE^{(g_s)}}{dt} \qquad [2.10c]$$

and

$$-\dot{E}_4 = -\frac{dE^{(g_n)}}{dt} \qquad [2.10d]$$

where $E^{(g_s)}$ and $E^{(g_n)}$ are given in Eqs. [2.6c] and [2.6d], respectively.

When all these terms are combined, we have

$$\dot{E}^{(\mu)} = -(\dot{E}_1 + \dot{E}_2 + \dot{E}_3 + \dot{E}_4)$$

demonstrating that the time rate of decrease of the four stored, or potential, energy components is equal to the rate of viscous dissipation. For two-dimensional systems on a homogeneous substrate, the fact that the total stored energy must be a nonincreasing function of time was shown by Mitlin (26) using variational methods. We will show that when the stored energy components are plotted versus time for mixed wettable systems, they shown characteristic patterns of alternating slow and rapid changes. Since the viscous dissipation rate is proportional to the square of the speed of motion, rapid decrease of potential energy corresponds to episodes of ''jumping'' motion. Alternating slow and rapid motions in two-dimensional systems have previously been reported (19).

In the following, we will present results using dimensionless variables. The reference state is a stationary paraboloidal drop with central height h_0 and radius R_0 lying on a flat substrate characterized by constant equilibrium contact angle θ_{e0}. Within the small slope assumption, the reference contact angle satisfies $\theta_{e0} \approx 2h_0/R_0$. The substrate coordinates are measured in units of R_0 [i.e., $(x, y) = R_0(\hat{x}, \hat{y})$], while film thickness h and wetting-layer thickness h_* are measured in units of h_0. The unit of energy is taken to be σh_0^2. Time is measured in units of

$$T^* = \frac{3\mu R^4}{\sigma h_0^3}.$$

With the hats discarded, the evolution equation, corresponding to Eqs. [2.1] becomes

$$h_t = -\nabla\cdot\left[h^3\left(\nabla\nabla^2 h + \frac{(n-1)(m-1)}{2h_*(n-m)} \times \nabla\left[C\left(\frac{h_*^n}{h^n} - \frac{h_*^m}{h^m}\right)\right] - Bo\cos\theta\nabla h\right)\right] + \frac{2Bo}{\theta_{e0}}\sin\theta(h^3)_x \quad [2.11]$$

and the energy components are

$$E_1 = \frac{1}{2}\iint \nabla h\cdot\nabla h dA, \quad [2.12a]$$

$$E_2 = \frac{1}{2}\iint C(x,y) \times\left[1 + \frac{m-1}{n-m}\left(\frac{h_*}{h}\right)^{n-1} - \frac{n-1}{n-m}\left(\frac{h_*}{h}\right)^{m-1}\right]dA, \quad [2.12b]$$

$$E_3 = \frac{Bo}{(h_0/R_0)}\sin\theta\iint x(h-h_*)dA, \quad [2.12c]$$

and

$$E_4 = \frac{1}{2}Bo\cos\theta\iint (h^2 - h_*^2)dA. \quad [2.12d]$$

The wetting function is

$$C(x,y) = \left[\frac{\theta_e(x,y)}{(h_0/R_0)}\right]^2 = 4\frac{\theta_e^2}{\theta_{e0}^2}. \quad [2.13]$$

Within the small-slope lubrication assumption, there is a degree of *similarity*. If gravity is neglected, viscosity and surface tension only appear in the time scale T^*. With gravity included, σ also appears in the Bond number

$$Bo = \frac{\rho g R_0^2}{\sigma}.$$

When the equilibrium contact angle is constant (i.e., $\theta_e = \theta_{e0}$), its actual value does not appear; for variable values of $\theta_e(x,y)$, the variation information is included in the specified function $C(x,y)$. A basic problem is the spreading behavior of an axisymmetric drop on a uniform substrate with gravity neglected. If the initial condition is paraboloidal, the only parameters that will appear in the model are the initial central height of the drop $h_c = h(r=0, t=0)$, and the wetting-layer thickness h_*, both measured in units of the final equilibrium height h_0.

3. NUMERICAL TECHNIQUES AND COMPUTATIONAL ISSUES

Equation [2.11] can be solved using finite-difference methods. It has the character of a higher-order diffusion equation and may be solved by marching in time. Diffusion equations can be treated by explicit techniques, as was done by us in early work (23). Much more efficient methods can be constructed, however.

The stability requirement for an explicit method is quite severe; it is easily shown, for the model equation

$$h_t = -h_{xxxx},$$

that the maximum permissible time step for stability Δt must be no larger than order Δ^4, where Δ is the space step or mesh size. Thus the computational requirement quickly becomes more severe as the mesh size becomes small. In the class of problems treated here, Δ must be comparable in size to the wetting-layer thickness h_* in dimensionless units, in order to maintain accuracy in the ''contact region'' where the macroscopic drop meets the wetting layer. For two-dimensional or axisymmetric problems in space, as in the next section, a semi-implicit method has been implemented. In this method, a system of linear equations for the increments in the vector of dependent variables h_i is solved at each time level. Nonlinear prefactors in [2.11] are evaluated at the old time level. The method may be made second-order-accurate in time by use of a predictor-corrector technique. Alternatively, it has been found that an adaptive time-stepping procedure, where the time step is adjusted dynamically based on a pre-set maximum permissible change in any h_i value, greatly increases computational efficiency. Temporal convergence can be verified by reducing the allowed change in h_i. Spatial steps as small as 10^{-4} have been used. This is sufficient resolution for the simulation to match experimental data on spreading drops, as will be seen later. For two-dimensional or axisymmetric problems, computational requirements are quite modest; depending on the value of h_* used, run times varied from less than 1 min for thick wetting layers to about 30 min for the thinnest layers, on a midlevel workstation. Using the semi-implicit method, run times are approximately proportional to the size of the vector h_i. The speed parameter $\Delta t/\Delta^4$, which measures the implicit/ex-

plicit speed ratio, can reach values as large as 10^8, during periods of slow shape evolution, when a fine mesh is used.

Numerical solution of three-dimensional cases, as in Section 5, also use finite difference methods and an alternating-direction-implicit (ADI) technique is implemented. Developed originally for second-order elliptic and parabolic systems (27), ADI uses alternating sweeps in each direction, and only a banded system of equations needs to be solved to update $h_{i,j}$ values in a row or column. A version of ADI called ''time-splitting'' has been applied to higher-order elliptic problems by Yanenko (28); similarly another variant, due to Conte and Dames (29), employs a predictor-corrector approach. We have used adaptations of both techniques, and they have similar performance. They each produce a high degree of stability; maximum permissible time steps can be as much as a factor of 10^5 larger than the characteristic maximum step for stability for the explicit method. For the spatially fourth-order system in Eq. [2.11], pentadiagonal systems need to be solved to update each row or column. Apparent contact lines are captured by the method and their motion appears as part of the evolving solution. There is no need to track or fit their position. This benefit is not without cost, however; computation needs to be performed over portions of the domain where only the thin, stagnant wetting layer is present. Further details of the unsteady simulation methods employed here are given by Moriarty and Schwartz (30) for axisymmetrical cases, and by Weidner *et al.* (31) where a three-dimensional problem is solved.

The shape of the disjoining energy well and the magnitude of the maximum gradients of the disjoining terms in Eq. [2.11] are controlled by the choice of the parameters (n, m) as well as h_*. For ''deeper'' wells, such as the (9, 3) case shown in Fig. 1b, a finer mesh needs to be used, for a given h_*. For $(n, m) = (3, 2)$ it was possible to use $h_* = 0.02$ for the three-dimensional cases, while, for the other choices, results are given only for $h_* = 0.04$. These wetting layers are not sufficiently thin to allow time-accurate simulation results. Thus a time-scale correction needs to be applied when comparing calculations to experimental observation, as explained and justified later. The three-dimensional cases use a 140 by 140 mesh with about 20,000 unknowns. Run times varied between from about 1 to 24 h, depending on the input parameter values.

4. AXISYMMETRIC SPREADING ON A UNIFORM PARTIALLY WETTING SUBSTRATE

As a preliminary study, we consider the axisymmetric spreading of a droplet on a uniform substrate and calculate $h(r, t)$ using Eq. [2.11] with $C = 4$. The droplet is assumed to be sufficiently small that gravity may be neglected. Since the equilibrium state is used as the reference for defining the dimensionless variables h and r, the final drop shape will be close to the paraboloid $h = 1 - r^2$. As an initial state, we use a much steeper droplet; the starting condition is the paraboloid

$$h(r, 0) = \mathrm{Max}[h_* + h_c(1 - h_c r^2), h_*]$$

where h_c is the initial centerline height, above the thin wetting layer h_*. The droplet volume, lying above h_*, is $\pi/2$ in dimensionless units, irrespective of the value of h_c. The evolution of the drop shape is tracked most simply by monitoring the central height $h(0, t)$. We start with $h(0, 0) = h_c = 10$ and show results for several choices of the constants h_*, m, and n. Calculated droplet shapes remain approximately paraboloidal as they spread and ultimately stabilize. In addition to determining specific information about spreading on low-energy substrates, a second goal is to determine the dependence of spreading speeds on wetting layer thickness h_*.

Figure 2 shows $h(0, t)$ plotted versus time for $h_* = 0.005$

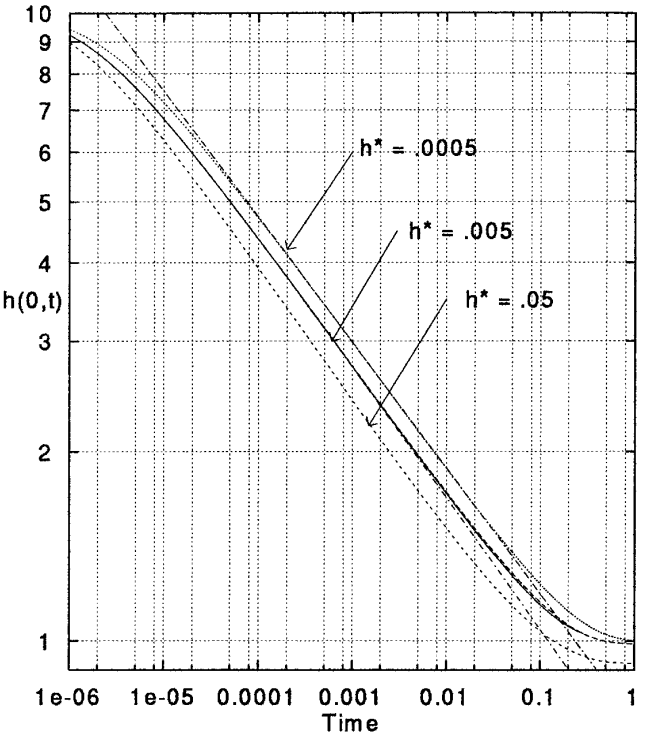

FIG. 2. Calculated values of the center height of a spreading axisymmetric liquid drop plotted versus time in dimensionless units. Logarithmic scales are used to show self-similar power-law behavior. Results are shown for three values of wetting-layer thickness h_*. For $h_* = 0.0005$, the calculated height variation agrees closely with the similarity solution $h = .75/t^{1/5}$ shown as a straight line. For all values of h_*, the disjoining exponent pair used is (3, 2). For $h_* = 0.005$, other calculations are also shown corresponding to the pair (9, 3) and the [perfect-wetting] pair (3, 1). The results overlap perfectly until $h(0, t)$ is almost equal to one, the stable equilibrium value. This is consistent with the experimental observations of Zosel (21).

and the disjoining exponent choices (n, m) equal to $(3, 2)$ and $(9, 3)$. For comparison, we also show the result for the perfectly wetting case, using the same program with $m = 1$. Note that taking $m = 1$ causes the disjoining term in the evolution equation to vanish. The two choices $(3, 2)$ and $(9, 3)$ are seen to be graphically indistiguishable. Moreover, they agree closely with the perfectly wetting or zero (equilibrium) contact-angle case until the droplet has almost stabilized. This is consistent with the experimental study of Zosel (21) who demonstrated, using various liquids and substrate materials, that droplet spreading is independent of the nature of the substrate until close to stabilization, on materials with a finite contact angle $\theta_e > 0$.

Logarithmic scales are used in Fig. 2 to show the essential power-law behavior of the spreading rate. Also shown in the figure are calculated results for two other values of h_*. For each h_*, results can be fitted, in the straight-line range, by

$$h(0, t) = \frac{K}{t^{0.2}}. \qquad [4.1]$$

This matches the calculated results over about three decades in time for $h_* = 0.005$ with $K = 0.68$. For $h_* = 0.05$, the droplet expands more rapidly, and the calculations shown are approximated, in the straight-line range, by taking K is equal to 0.61. Similarly, for $h_* = 5 \times 10^{-4}$, the best-fit slope is obtained with $K = 0.75$. Equation [4.1] with $K = 0.75$ is shown as a straight line in the figure. This power-law behavior is sometimes referred to as Tanner's law (12) and was verified experimentally by him and others for thin droplets expanding on high-energy substrates ($\theta_e \approx 0$). It is indicative of the existence of a *self-similar solution* to the problem which is achieved a short time after the start of the motion, when the details of the initial shape are no longer important.

Self-similarity may be established by the following argument. Away from equilibrium, the capillary pressure in the drop is higher by a factor of approximately $[h(0, t)/h_0]^2$. This ratio is a measure of the relative importance of the capillary and disjoining terms in the evolution equation. It is only when the ratio approaches one that the disjoining term will be felt. Thus, except near equilibrium, spreading is governed by a balance of surface tension and viscous forces; the equation, in dimensionless variables, is simply

$$h_t = -\nabla \cdot h^3(\nabla\nabla^2 h). \qquad [4.2]$$

A similarity solution is sought in the form

$$h(r, t) = t^{\beta} f\left(\frac{r}{t^{\alpha}}\right) = t^{\beta} f(\eta) \qquad [4.3]$$

where η is the similarity variable and α and β are constant exponents. Volume V will be conserved provided

$$V = 2\pi t^{\beta+2\alpha} \int_0^{R/t^{\alpha}} f(\eta)\eta d\eta$$

is independent of time. $R(t)$ is the sensible radius of the drop, located near, but not including, the contact region. Time independence will be achieved if

$$\beta + 2\alpha = 0$$

and if R is proportional to t^{α}. Now substituting Eq. [4.3] in Eq. [4.2] and performing the indicated differentiations using the chain rule yields

$$\beta t^{\beta-1}[f + (\eta/2)f'] = t^{6\beta}\frac{1}{\eta}\left[\eta f^3\left[\frac{1}{\eta}(\eta f')'\right]'\right]' \qquad [4.4]$$

where $(')$ denotes $d/d\eta$. Separate dependence on t is now removed if

$$\beta = -\frac{1}{5} \qquad [4.5a]$$

and

$$\alpha = \frac{1}{10}. \qquad [4.5b]$$

Equation [4.4] may be integrated once; the constant of integration must be zero in order that the droplet profile be smooth at $r = 0$ for all time. The resulting third-order nonlinear ordinary differential equation for $f(\eta)$ is

$$f''' + \frac{f''}{\eta} - \frac{f'}{\eta^2} = \frac{\eta}{10 f^2} \qquad [4.6]$$

The solution to Eq. [4.6] represents the profile shape away from the contact region. Near the drop margins, its solution behaves like the solution to $f''' = \text{const}\, f^{-2}$, the equation appropriate to the so-called intermediate region for the steady two-dimensional spreading problem treated by Tuck and Schwartz (13).

It suffices here to recognize that

$$h = t^{-1/5} f\left(\frac{r}{t^{1/10}}\right) \qquad [4.7]$$

and that the entire family of profiles, in the self-similar re-

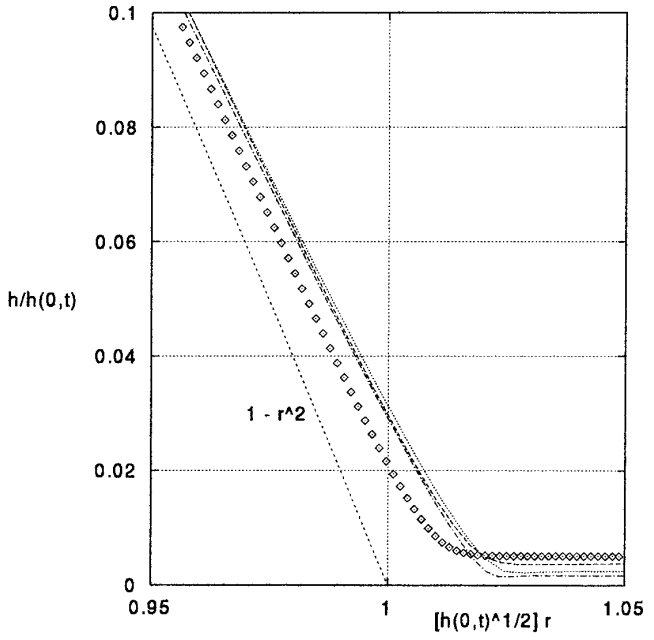

FIG. 3. Contact region of a spreading axisymmetric drop. The profiles for $h(0, t) = 1.25$, 2, and 3 are clustered together showing similarity when $h(r, t)/h(0, t)$ is plotted versus $h(0, t)^{1/2}r$. The final steady profile is plotted with points. For comparison, the paraboloid $h = 1 - r^2$ is also shown. The disjoining exponent pair is (3, 2) and $h_* = 0.005$ for each calculated profile.

gime, may be collapsed onto a single curve by plotting them as

$$\frac{h}{h(0, t)} = f(h(0, t)^{1/2}r).$$

This is shown in Fig. 3 where profiles are shown for three times, corresponding to different values of $h(0, t)$ in the self-similar rangle. The final droplet shape and the paraboloid $h = 1 - r^2$ are also shown for comparison. Only the contact region is shown since for most of the drop, the various curves are almost indistinguishable. While the power-law exponents were given first by Tanner, the fact that the entire profile is self-similar, while implicit in his analysis, does not appear to have been recognized.

When the dimensions are restored to Eq. [4.1], it becomes

$$\frac{h(0, t)}{h_0} = \frac{R_0^2}{R^2} = \frac{1}{K}\left(\frac{\sigma h_0^3 R_0^6 t}{3\mu}\right)^{1/5} \qquad [4.8]$$

where h_0 and R_0 are the reference height and radius of the final stabilized droplet. Since the initial droplet was taken to be a paraboloid, the volume $V = (\pi/2)h_0R_0^2$. When inserted in Eq. [4.8], a formula for the area A of the expanding droplet on the substrate is obtained as

$$A = \pi R^2 = \frac{1.923}{K}\left(\frac{\sigma V^3 t}{\mu}\right)^{1/5}. \qquad [4.9]$$

Lelah and Marmur (14) measured the rate of expansion for water droplets on glass. They offer a best-fit correlation of their data as

$$A = 12V^{.6}t^{.2} \qquad [4.10]$$

using cgs units with $\sigma = 72$ dyn/cm and $\mu = 0.01$ poise. However their data show significant scatter, and there is a rather strong dependence on relative humidity. Humidity may plausibly be correlated with the dimension of a thin ambient wetting layer on the glass. Teletzke *et al.* (17), in their theoretical study, but employing previously taken experimental data, predict a value of 15 for the constant in [4.10] for water on glass. By comparison, we find, using the value $K = 0.68$, appropriate to the dimensionless wetting film thickness $h_* = 0.005$, the constant in Eq. [4.10] to be 16.7. For $h_* = 5 \times 10^{-4}$, $K = 0.75$ and the constant is 15.1, close to the value of Teletzke *et al.* Using this latter value, and taking midrange measurements from Lelah and Marmur (14), the nominal wetting film thickness is roughly 30 nm, which seems a plausible value.

The preceding rather credible agreement between the spreading laws masks a much larger sensitivity. Spreading speeds must be compared at equivalent drop positions, rather than at similar times. Differentiating Eq. [4.1] with respect to time, one obtains

$$h_t = -\frac{K}{5t^{6/5}} = -\frac{h^6}{5K^5}. \qquad [4.11]$$

Since the droplet expansion rate R_t is proportional to $-h_t$, the spreading rate is proportional to K^{-5}. Using the previous calculated results, for example, changing h_* by two orders of magnitude, from 5×10^{-2} to 5×10^{-4}, reduces the spreading rate by a factor of about 2.8.

In order to maintain computational accuracy, we find that the point spacing in the finite-difference method Δ must be no greater than h_*. Thus the computational requirements become much greater as h_* is reduced. Unlike the axisymmetric case just treated, in the three-dimensional simulations discussed later, the computational problem is much larger, and it is not possible to have a mesh sufficiently fine to allow very small h_* values. The h_* values used in three-dimensional simulation will be too large by a factor of 100 or more. Consequently, the speed of motion will be overpredicted by a factor of about three from this effect alone.

The speed variation with h_* found earlier may be compared with a simple analytical estimate. Assume that a force per unit contact-line length F is available to drive the motion which proceeds at speed U. F is balanced by the integrated shear stress on the substrate

$$\int \tau(0)dx = 3\mu U \int \frac{dx}{h} = \frac{3\mu U}{\theta_e} \int \frac{dh}{h},$$

using $dh/dx \approx \theta_e$ which is appropriate to the wedge-shaped contact region where most of the viscous work is done. If the limits of integration on h are h_* and some h_1, we obtain simply

$$F = \frac{3\mu U}{\theta_e} \log\left(\frac{h_1}{h_*}\right).$$

Here h_1 is a macroscopic length that is assumed constant as $h_* \to 0$. If we identify h_1 with h_0, for example, the predicted change in U, due to a change in h_*/h_0 from 2×10^{-2} to 2×10^{-4} is a factor of 2.53, in reasonable agreement with the factor of 2.8 found previously.

5. SPONTANEOUS MOTION ON A WETTABILITY CROSS

Three-dimensional numerical simulations have been performed for a droplet moving on a substrate composed of two different materials. The specific geometry, chosen to model the experimental results given later, is a uniform substrate upon which lies a cross of higher contact angle material. In the experiment, the liquid is glycerin and the substrate is a Teflon cross applied onto a glass slide. The starting condition for the simulation is a paraboloidal drop placed near the center of the cross. Three different choices for the disjoining pressure functional have been used. The reference state, used to specify h_0 and R_0, is a static drop at equilibrium on the smaller contact angle (higher substrate energy) material. In all simulations, the width of each stripe of the cross is taken to be one-quarter of the nominal droplet radius R_0. The substrate is horizontal. Gravity is neglected entirely for most of the results given here. It is included in one case, however, in order to ascertain its effect, which is found to be rather small. Two different values of h_* have been used, 0.02 and 0.04, expressed as fractions of h_0. The mesh size is 0.025 R_0, and the computational domain is of size 140×140. The contact angle is three times larger on the cross than on the surrounding field, leading to a factor of nine difference in the wettability function C in Eq. [2.11]. In order to make C differentiable, a cubic polynomial smoothing function is applied at substrate material boundaries. The width of this smoothing region is $0.05R_0$ on each side of the material boundary.

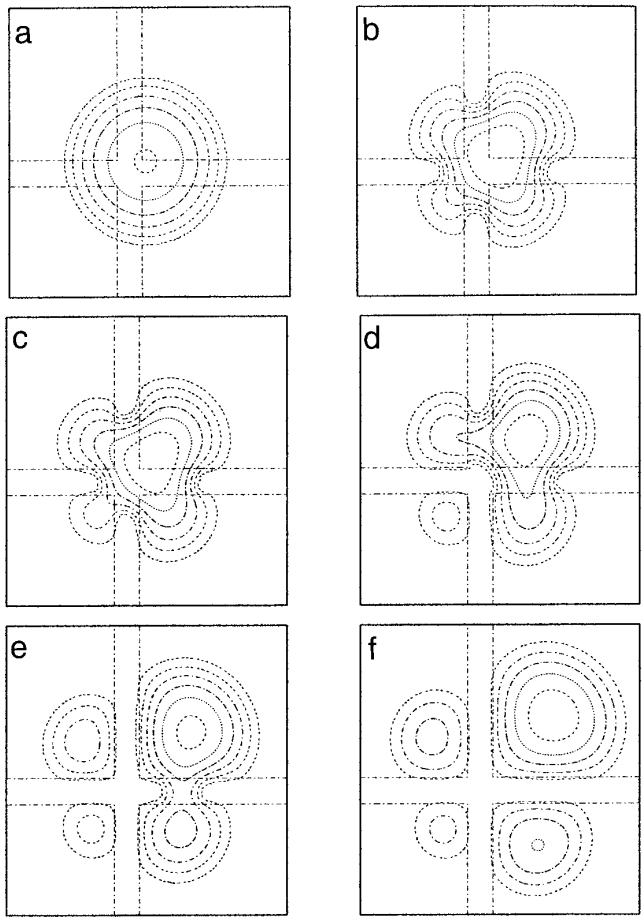

FIG. 4. Contour plots for droplet placed near the center of a ''cross'' of high-contact-angle material. Dimensionless times are (a) $t = 0$, (b) $t = 0.1$, (c) $t = 0.2$, (d) $t = 0.35$, (e) $t = 0.5$, and (f) $t = 0.7$. Contour levels are 0.025, 0.2, 0.4, 0.6, 0.8, and 1.0. Disjoining exponents are (3, 2) and $h_* = 0.02$.

Contour plots of the droplet shape at six different times are given in Fig. 4. The disjoining exponent pair is (3, 2) and $h_* = 0.02$. Initially, in this and all other runs, the droplet is displaced a vector distance $(0.2R_0, 0.14R_0)$, upward and to the right, from the cross center as shown in Fig. 4a. The droplet quickly contracts inward along the high-contact-angle cross and the central height increases (Fig. 4b). By (dimensionless) time $t = 0.2$ in Fig. 4c the drop has shifted noticeably upward and to the right, and the disconnection of the small region in the lower left quadrant has begun. At $t = 0.35$ (Fig. 4d), the small droplet has separated completely and the next, somewhat larger drop, at the upper left is beginning to pinch off. This second disconnection is completed by $t = 0.5$ (Fig. 4e) and the last drop break is in progress. The four isolated droplets are shown at a later time $t = 0.7$ in Fig. 4f. From this point on, motion proceeds

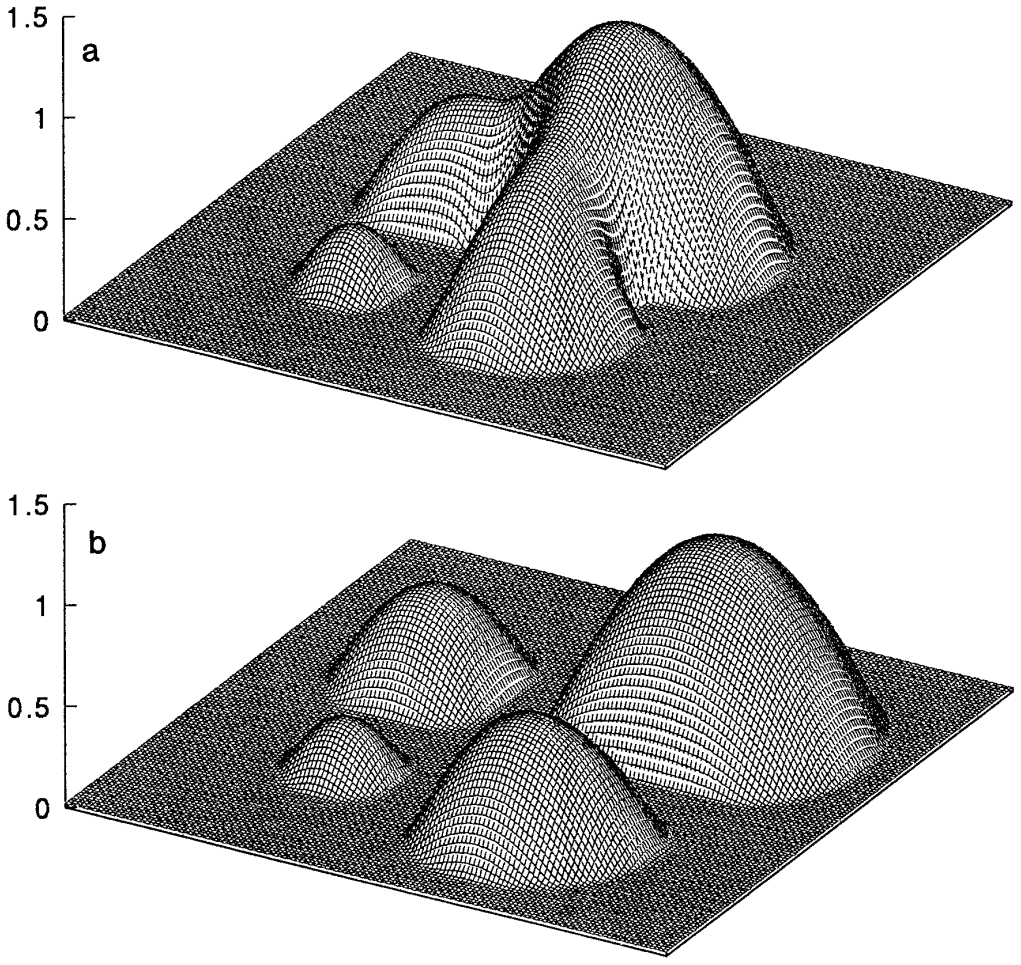

FIG. 5. Wire cage pictures of drop shapes at two values of dimensionless time. (a) $t/T^* = 0.35$; (b) $t/T^* = 0.70$.

very slowly as each drop moves away from the wettability boundaries in order to reduce its surface area by becoming more circular. Figure 8a shows the result of this slow motion at $t = 1.0$.

Wire-cage pictures are helpful in visualizing the drop shapes. Figure 5 shows pictures from the same run for $t = 0.35$ and $t = 0.7$. These correspond to the contour plots in Figs. 4d and 4f, respectively. Apparent contact angles, where the drop portions appear to meet the substrate, vary widely, even upon the same substrate material. It appears that local contact angles are greater in places where the margins are advancing rapidly and smaller at receding edges. However, the idea, that has sometimes been advocated, that dynamic contact angles are solely determined by, or can be correlated with, local conditions such as speed, is clearly an oversimplification. It is appropriate only in situations with a high degree of symmetry, such as an axisymmetric spreading drop. The mathematical character of the governing equations is essentially elliptical; thus all regions of the drop contribute somewhat to conditions at a given location.

The energy components derived in Section 2 are plotted versus time in Fig. 6 for the simulation shown in Figs. 4 and 5. The indicated surface and substrate energies correspond to the dimensionless energies E_1 and E_2 from Eqs. [2.12a] and [2.12b]. The total energy is seen to be monotonically decreasing, as it must be, since its negative, the viscous dissipation rate, is inherently positive. From the energy plots, it is possible to see each disconnection event quite clearly. They correspond to regions of large slope since the disconnections occur rapidly. There are four regions of large slope on each curve in Fig. 6. They are the initial inward contraction of the meniscii on the cross, which happens almost immediately, followed by the three drop breaks. The slopes, during the rapid events, are about ten times larger than the average rate of decrease of the total energy. This alternation of slow and rapid events seems characteristic of motions on mixed-wettable substrates. It is reminiscent of the commonly observed ''jumpy'' motion of raindrops on a dirty window pane, for example. Near the end of the motion, at $t/T^* = 1$, the substrate and surface energies are in the approximate

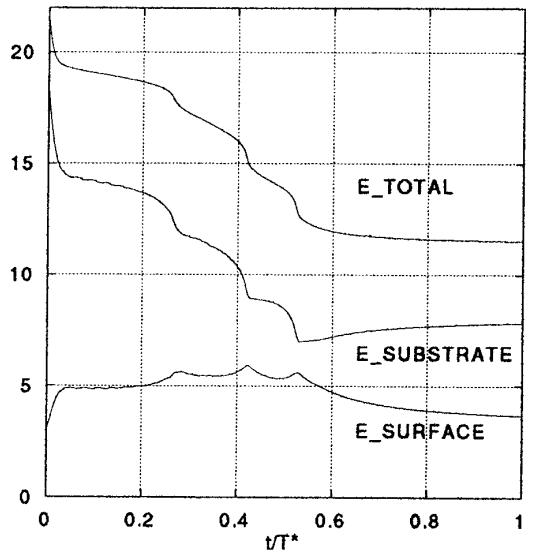

FIG. 6. Energy components versus time; Disjoining exponents are (3, 2); $h_* = 0.02$.

ratio 2:1 which was predicted for a paraboloidal drop at equilibrium on a uniform substrate in Eqs. [2.8a] and [2.8b]. This ratio holds for a set of discrete drops as well.

Figure 7 shows the variation in energy components with time when gravity is included in the simulation. The gravitational energy is calculated using Eq. [2.12d], with the inclination angle θ equal to zero. The Bond number $Bo = \rho g R_0^2/\sigma$ is 2.5, using the density and surface tension of glycerin used in the experiment. The radius is $R_0 = 0.4$ cm. The gravitational component is seen to be smaller than the others.

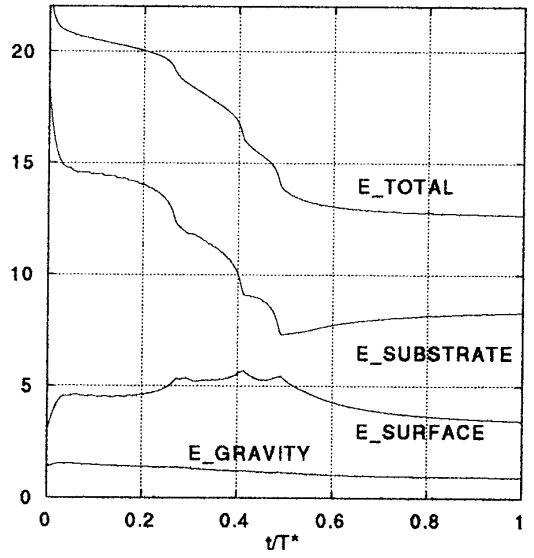

FIG. 7. Energy components versus time with gravity effect included; Bond number $Bo = 2.5$; Disjoining exponents are (3, 2), $h_* = 0.02$.

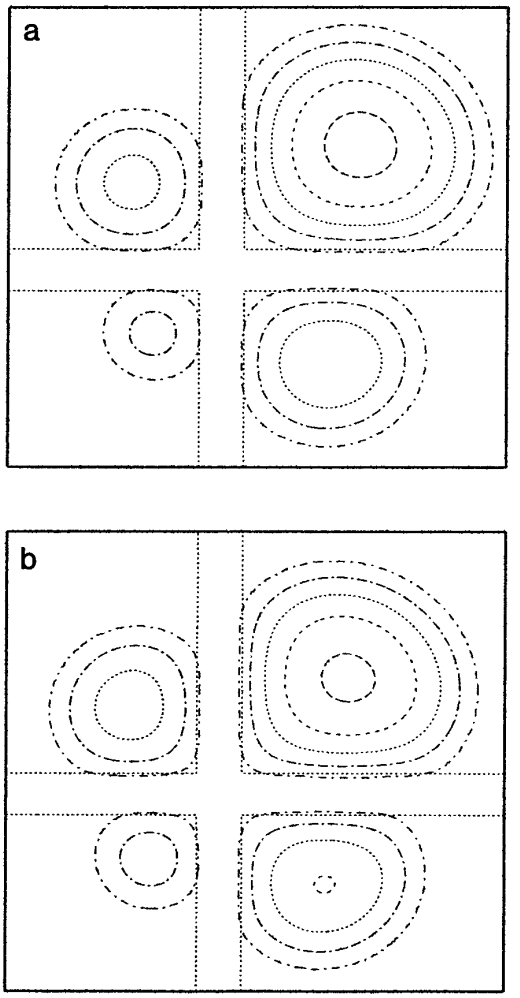

FIG. 8. Comparison of separated droplet shapes at $t/T^* = 1$ to ascertain the effect of gravity. (a) No gravity. (b) Gravity is included; Bond number $Bo = 2.5$. Contour levels are 0.025, 0.2, 0.4, 0.6, and 0.8. Disjoining exponents are (3, 2) and $h_* = 0.02$.

After a slight initial rise as the drop contracts on the cross, it falls monotonically with a gentle slope. The disconnection events are virtually identical to the case when gravity is excluded. The major effect, seen by comparing Figs. 6 and 7, is a reduction in the time scale, or speed-up, with gravity included, of about 5%. Figure 8 compares contours without gravity (Fig. 8a), and with gravity included (Fig. 8b) at time $t/T^* = 1$. They are quite similar, but careful examination shows that the liquid is a bit more evenly distributed among the four droplets when gravity is included. This is consistent with the slightly earlier times for the break-up events. The disproportioning is caused by the slow drift of the initial drop to the upper right; the earlier the disconnections occur, the more uniform will be the size distribution of the four drop fragments.

Figure 9 considers the effect of the choice of disjoining

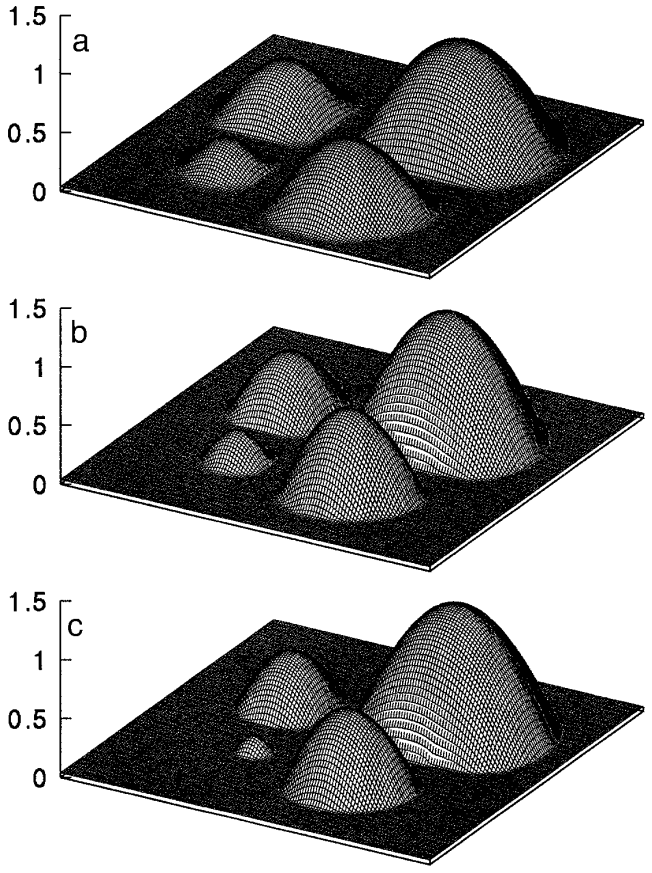

FIG. 9. Effect of the disjoining pressure function on the final drop pattern. $h_* = 0.04$ and the (n, m) values are (a) (3, 2); (b) (4, 3); (c) (9, 3).

pressure function. Each part of the figure shows the droplet fragments after final disconnection. The disjoining pressure exponents are (a) (3, 2), (b) (4, 3), and (c) (9, 3). In all three cases, the wetting layer thickness used was $h_* = 0.04$. The major observed difference between the three is the relative size of the fragments, especially the smallest droplet in the lower left corner. The energy wells, from Fig. 1b, are progressively steeper as we go from case a to case c. This results in increasing ''stiffness'' of the drops and consequent greater translation of the large initial drop before break-up occurs. Break-up is a more efficient mechanism for energy reduction than gross translation, but it is resisted by drop stiffness. The calculated times for the final drop disconnection for the three cases are $t/T_* =$ (a) 0.39, (b) 0.46, and (c) 0.74. From Fig. 6, where $h_* = 0.02$, this time is 0.53. Since there is significant uncertainty in the initial condition for the experiment, more important are intervening time periods between the three droplet breaks. From Fig. 6, these are seen to be 0.15 and 0.10. The corresponding numbers for the simulations shown in Fig. 9, where $h_* = 0.04$, are (a) (0.12, 0.08) for the exponent pair (3, 2); (b) (0.13, 0.09) for the pair (4, 3); (c) (0.24, 0.11) for (9, 3). For the (3, 2) pair, the reduction in these time intervals, caused by the factor of two increase in h_*, is 20–25%. This is consistent with the predicted dependence on h_* examined, for axisymmetric spreading, in Section 4. The speed difference appears to be the major effect of changes in h_*. It may be observed that the profiles in Figs. 5b and 9a are very similar.

An experiment has been performed which can be compared with the computations. A cross of 0.1 cm wide Teflon tape was applied to a glass slide. A droplet of glycerin was placed near the center of the cross. The droplet volume was 23 μl; glycerin viscosity is $\mu = 9.5$ poise, and the surface tension is $\sigma = 63$ dyn/cm. The subsequent droplet motion, including the break-up events, was recorded using a CCD camera. The average droplet radius near the start of the motion was observed to be about four times the stripe width. Using the value $R_0 = 0.4$ cm and the known value of volume, and assuming a paraboloidal drop, the central height of the nominal axisymmetric drop is calculated to be $h_0 = 0.091$ cm. The time scale $T^* = 3\mu R_0^4/(\sigma h_0^3)$ is 15.5 s using these values. Separate static measurements of isolated drops of glycerin on glass and the Teflon material showed contact angles of 38° and 114°, respectively. Thus a factor of three difference between contact angles was chosen for the numerical simulation. It is noted that these large contact angles, particularly the one for Teflon, are beyond the range of validity of the small-slope lubrication approximation. Thus only qualitative or semiquantitative agreement between experiment and theory can reasonably be expected.

Several frames from the movie are shown in Fig. 10. The time, in seconds, after drop deposition is given for each frame. White dots have been added to help visualize the drop edges. The Teflon cross is shown, along with the edges of the drop including the meniscii on the cross. Optical distortion of the straight Teflon tape can be seen on that portion of the tape covered by the liquid. This is a diffraction effect because the drop acts as a lens. The initial frame ($t = 2.5$ s) already shows the liquid retracting on the stripes; this continues into the second frame taken at $t = 10$ s. By $t = 35$ s, the first disconnection has occurred, and the retracted meniscus passes through the center of the cross. The frame at $t = 50$ s shows two separated droplets; this picture is similar to the simulation picture in Fig. 4e at the dimensionless time $t/T^* = 0.50$. The three drop disconnection times, taken from the movie, are about 32, 39, and 55 s.

Qualitative features of the theory given here are confirmed by the experiment. The most important conclusion is that the incorporation of substrate wettability variation into a contact angle function in the evolution equation is sufficient to produce realistic wetting/dewetting behavior. Comparison with the simulation results of Fig. 4 suggests that the characteristic time T^* should be about 100 s, about seven

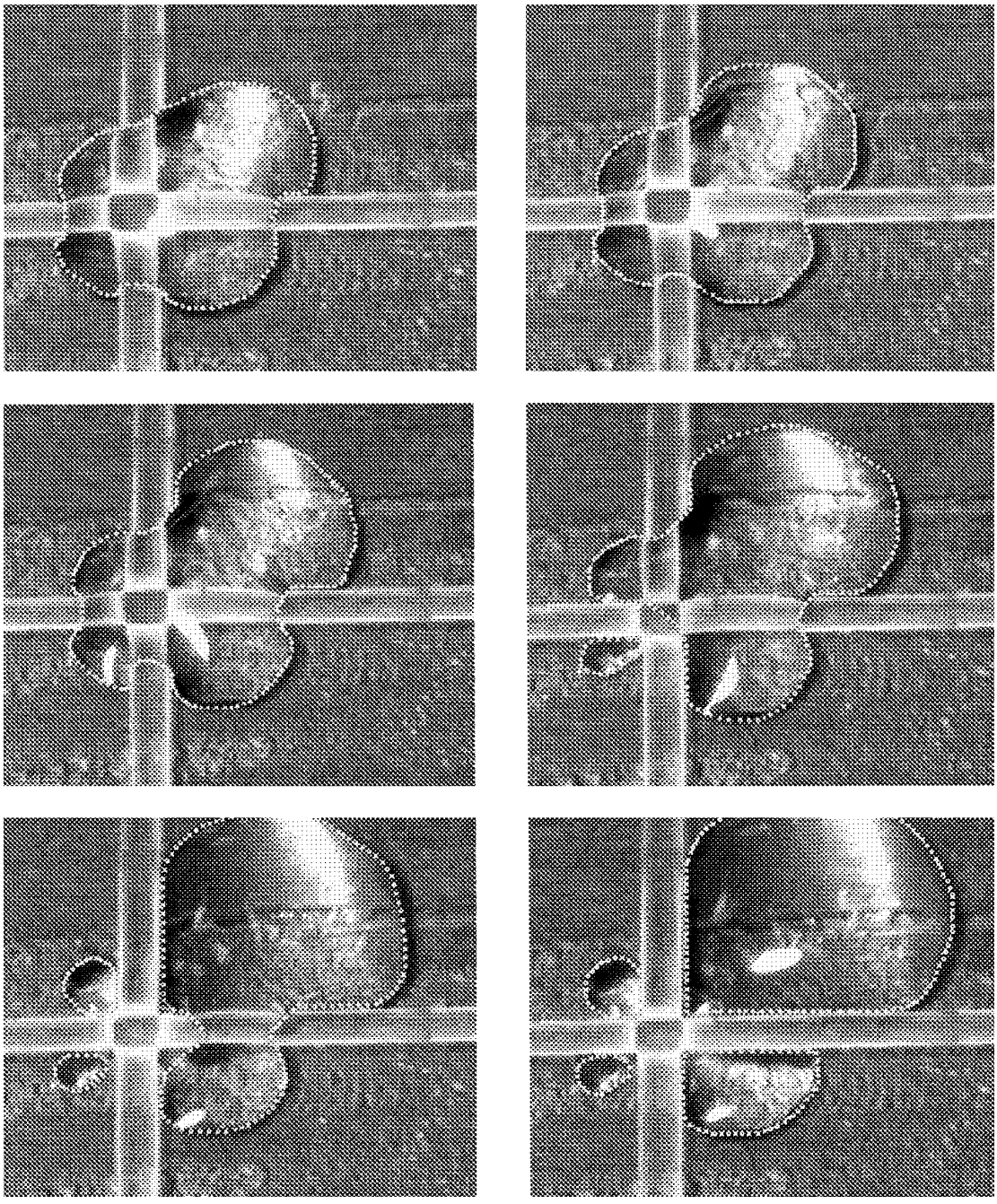

FIG. 10. Video images taken from an experiment where a glycerin drop is placed near the center of a cross of 0.1 cm Teflon tape on a glass slide. These pictures may be compared with the simulation shown in Fig. 4. Reading across, then down, the times are 2.5, 10, 22, 35, 50, and 70 s.

times larger than the calculated value. The principal cause of this difference is the too-large value of h_*, the wetting-layer thickness used in the simulation. In dimensional terms, h_* used in the calculation is (0.02) (0.091 cm) = 18.2 μm. The analysis of Section 4, where comparison is made to experimental results for spreading of water drops on glass, suggests that h_* is too large by perhaps a factor of 500. Numerical and analytic estimates made in that section indicate that speeds will be too large by a factor of about three from that cause alone.

There are three factors which contribute to the remaining speed discrepancy, which is a factor between two and three. These are (i) the overly large values of contact angle compared with the limitations of the small-slope lubrication the-

ory. In particular, the use of $\nabla^2 h$ for the droplet curvature, rather than the exact expression, results in an overprediction of the driving capillary pressure within the drop by a factor that approaches two as the contact angle approaches 90°. (ii) Either physical or chemical heterogeniety on the nominally clean uniform substrates, if present, can be expected to slow down the motion. (iii) Had the comparison been made with the (9, 3) disjoining law rather than the (3, 2) law, simulation time intervals would have been longer. The calculations leading to Fig. 9 indicate that this factor is almost two. Indeed, each of the disjoining laws used in the simulations of Fig. 9 is a plausible candidate to match the experimental data. Had the initial offset of the drop, an arbitrarily selected quantity, been taken a bit smaller, the simulation using (9, 3) would have resulted in more uniform fragment volumes.

6. CONCLUSIONS

A mathematical and computational model has been presented that allows the calculation of the unsteady motion of droplets on heterogeneous substrates. By assigning different values of the equilibrium contact angle to particular substrate regions, droplet motion on chemically contaminated surfaces may be modeled. Realistic-looking wetting/dewetting behavior including droplet break-up has been calculated. The motion proceeds by alternating fast and slow events in a ''jumpy'' fashion, corresponding to familiar observation. For a particular pattern of wettability, a simple experiment has been performed that qualitatively confirms the features predicted by the numerical model.

For the simpler problem of axisymmetric droplet speading on a uniform substrate, the effect of finite contact angle has been shown to be limited to those late times when the droplet has almost stabilized, in agreement with the observations of Zosel (21). These simple solutions have also identified the magnitude of the wetting-layer thickness needed in the simulation in order to match experimental spreading rates. The axisymmetric spreading results have also been used to verify three-dimensional calculations. An axisymmetric, or slightly perturbed, initial drop spreads until it ultimately stabilizes near the equilibrium contact angle. This may be compared with the stability result for a *uniform* layer of thickness h_1 on a homogeneous substrate. Using the present disjoining pressure model, it is easy to show that a uniform layer is unstable, if the conditions $m > 1$ and $h_1/h_* > (n/m)^{1/(n-m)}$ are satisfied, and that the total stored energy will be reduced if the surface becomes undulatory. For a developed drop of given volume, on the other hand, the nominally dry region is already at its energy minimum. Axisymmetric spreading is the most efficient method of energy reduction for the drop and surface tension quickly removes any perturbations to the initial shape; this is consistent with experimental observation (14, 21). The final equilibrium, with all the volume in a single rather than multiple drops, is clearly a global energy minimum for the system. Thus for the drop-on-cross problem considered here, the sole mechanism for break-up is the wettability contrast rather than instability.

The influence of the submicroscopic physics at the wetting line has been incorporated by use of a disjoining term in the evolution equation; the effects of changes in this term have been examined. It is thus possible, in principle, to use observed macroscopic motions of droplets and other liquid films as a probe of these mechanisms. In order for this goal to be realized, however, more carefully controlled experiments than the one presented here will be required. Material systems can be selected so that static contact angles lie within the range of applicability of lubrication theory.

The microscopic origins of contact angle hysteresis and the relation to specific wettability patterns can be better understood using the model. The hysteretic effect has long been recognized to be associated with multiple energy minima in the substrate energy function. Thus wetting lines can be trapped in different positions depending on the previous history of the motion. Quasi-static analyses that calculate and compare the energetics of liquid regions on striped substrates have appeared for one-dimensional and axisymmetric substrate patterns (32, 33). These were extended to two-dimensional patterns; more complicated wetting-line shapes were produced which were then confirmed experimentally. Discontinuous or ''jumping'' events were also predicted using the static theory (34, 35). Unlike the present work, these analyses take no account of the dynamics of flow. Whether or not a local energy barrier will successfully trap a liquid volume depends on the full liquid configuration; depending on the speed of the motion, the configuration may be far from equilibrium and may hence be sufficiently energetic to overcome the barrier. The present formulation is well-suited to answer questions such as these; moreover it is easier to apply than the static methods, since wetting lines are captured by the solution, rather than having to be explicitly fitted at each instant of time.

Answers to these questions have application in many areas. Prediction of wetting/dewetting behavior on heterogeneous surfaces is needed in the coatings, oil-extraction, and other industries. Another interesting application is the control of liquids in the microgravity environment of space. In the absence of gravity, wetting forces are especially important. On a very much smaller scale, Greenspan (10) considers the analogy between droplet motion and the motion of a cell. He states that an important objective in the understanding of cell motility is to differentiate between phenomena that depend on inanimate fluid mechanisms, such as those considered here, and ''those extraordinary cell processes that characterize life.''

There are limitations associated with straightforward im-

plementatation of the present approach, however. Resolution of wetting-layer thicknesses in the nanometer range is not possible for multidimensional problems; nor it is practically possible to resolve substrate variations on the micron scale, in macroscopic simulations. This is due entirely to current limitations on computer size and speed. It is anticipated, therefore, that asymptotic mathematical solutions will need to be used to extrapolate the present results down to such small scales.

The Frumkin–Deryaguin model (5–7) used here is not the only choice for representing the effect of intermolecular forces for partially wetting systems. Ruckenstein and coworkers (36, 37) consider a balance of liquid–liquid and liquid–solid interaction forces near a contact line and find an expression for the static contact angle in terms of the elemental force-law constants. Recent studies of fluid motion employ this expression (38, 39); the resulting small-slope evolution equation uses a term of the form

$$\text{const}\ \frac{h_x^4 - \theta_e^4}{h^3} \qquad [6.1]$$

instead of Eq. [2.2]. Since this term must remain bounded as $h \to 0$, one has $|h_x| \to \theta_e$ in that limit. Using either model, θ_e is the apparent contact angle at rest. The model in Eq. [6.1] is equally capable of representing substrate heterogeniety $\theta_e(x, y)$. For contact line motion, some additional provision must still be made to relieve the viscous stress singularity. This may be accomplished by use of a precursor layer, as used here, or by introduction of a slip coefficient (11, 39, 40). A numerical demonstration of the equivalence of these two approaches has been given for a particular problem, the two-dimensional steady gravity drainage of a wetting film on a vertical wall (13). While Eq. [6.1] is a good candidate for further study, it needs to be demonstrated that it can be made compatible with the efficient ADI numerical method and contact line ''capturing'' approach used here.

ACKNOWLEDGMENTS

This work is supported by the ICI Strategic Research Fund, the NASA Microgravity Program, and the State of Delaware. The authors also thank a referee for suggesting the use of Eq. [6.1].

REFERENCES

1. Dussen, V., E. B., *Ann. Rev. Fluid Mechanics* **11,** 371 (1979).
2. Benney, D. J., *J. Math. Phys.* **45,** 150 (1966).
3. Atherton, R. W., and Homsy, G. M., *Chem. Eng. Comm.* **2,** 57 (1976).
4. Chang, H. C., *Ann. Rev. Fluid Mechanics* **26,** 103 (1994).
5. Frumkin, A. N., *Zh. Fiz. Khim.* **12,** 337 (1938).
6. Deryaguin, B. V., *Zh. Fiz. Khim.* **14,** 137 (1940).
7. Churaev, N. V., and Sobolev, V. D., *Adv. Colloid Interface Sci.* **61,** 1 (1995).
8. Mohanty, K. K., Ph.D. Dissertation, Univ. of Minnesota, 1981.
9. Huh, C., and Scriven, L. E., *J. Colloid Interface Sci.* **35,** 85 (1971).
10. Greenspan, H. P., *J. Fluid Mechanics* **84,** 125 (1978).
11. Hocking, L. M., *Quart. J. Mech. Appl. Math.* **34,** 37 (1981).
12. Tanner, L., *J. Phys. (D)* **12,** 1473 (1979).
13. Tuck, E. O., and Schwartz, L. W., *SIAM Rev.* **32,** 453 (1990).
14. Lelah, M. D., and Marmur, A. M., *J. Colloid Interface Sci.* **82,** 518 (1981).
15. Starov, V. M., Kalinin, V. V., and Chen, J.-D., *Adv. Colloid Interface Sci.* **50,** 187 (1994).
16. Williams, M. B., and Davis, S. H., *J. Colloid Interface Sci.* **90,** 220 (1982).
17. Teletzke, G., Davis, H. T., and Scriven, L. E., *Chem. Eng. Comm.* **55,** 41 (1987).
18. Kheshgi, H. S., and Scriven, L. E., *Chem. Eng. Sci.* **46,** 519 (1991).
19. Mitlin, V. S., and Petviashvili, N. V., *Phys. Lett. A* **192,** 323 (1994).
20. Jameel, A. T., and Sharma, A., *J. Colloid Interface Sci.* **164,** 416 (1994).
21. Zosel, A., *Colloid Polym. Sci.* **271,** 680 (1993).
22. DeGennes, P. G., *Rev. Mod. Phys.* **57,** 827 (1985).
23. Schwartz, L. W., *Phys. Fluids* **A1,** 443 (1989).
24. Mitlin, V. S., *Colloids Surf.* **89,** 97 (1994).
25. Schwartz, L. W., *Proc. 3rd Micrograv. Fluid Phys. Conf.,* NASA CP 3338, 609 (1996).
26. Mitlin, V. S., *J. Colloid Interface Sci.* **156,** 491 (1993).
27. Peaceman, D. W., and Rachford, H. H., *SIAM J.* **3,** 28 (1955).
28. Yanenko, N. N., ''The Method of Fractional Steps.'' Springer-Verlag, New York, 1971.
29. Conte, S. D., and Dames, R. T., *Math. Tables Aids Comput.* **12,** 198 (1958).
30. Moriarty, J. A., and Schwartz, L. W., *J. Colloid Interface Sci.* **161,** 335 (1993).
31. Weidner, D. E., Schwartz, L. W., and Eres, M. H., *J. Colloid Interface Sci.* **187,** 243 (1997).
32. Johnson, R. E., and Dettre, R. H., *J. Phys. Chem.* **68,** 1744 (1964).
33. Neumann, A. W., and Good, R. J., *J. Colloid Interface Sci.* **38,** 341 (1972).
34. Schwartz, L. W., and Garoff, S., *Langmuir* **1,** 219 (1985).
35. Schwartz, L. W., and Garoff, S., *J. Colloid Interface Sci.* **106,** 422 (1985).
36. Miller, C. A., and Ruckenstein, E., *J. Colloid Interface Sci.* **48,** 368 (1974).
37. Ruckenstein, E., and Dunn, C. S., *J. Colloid Interface Sci.* **59,** 135 (1977).
38. Kalliadasis, S., and Chang, H.-C., *Ind. Eng. Chem. Res.* **35,** 2860 (1996).
39. Hocking, L. M., *Phys. Fluids* **A5,** 793 (1993).
40. Hocking, L. M., *Phys. Fluids* **6,** 3224 (1994).